Appl. Phys. B 27, 115–122 (1982)

Applied Physics B Photophysics and Laser Chemistry

Vibrational Relaxation of Dye Molecules Investigated by Ultrafast Induced Dichroism

D. Reiser and A. Laubereau

Physikalisches Institut der Universität, D-8580 Bayreuth, Fed. Rep. Germany

Received 10 December 1981/Accepted 21 December 1981

Abstract. Theoretical and experimental data are presented on the propagation of picosecond pulses in weakly excited dye solutions. It is shown that the so called "coherence peak" of the induced dichroism observed at short delay times depends on the vibronic relaxation and the excited state absorption of the dye molecules. Interpretation of the experimental results is considerably facilitated at low excitation level. The vibrational relaxation time in the S_1 state of phenoxazone 9 was measured to be $\tau_v = 0.8 \pm 0.3$ ps, 0.7 ± 0.2 ps and 0.7 ± 0.2 ps, respectively, for the solvents dioxane, solid polystyrene and CCl_4. For rhodamine 6 G in ethanol we find $\tau_v = 0.5 \pm 0.2$ ps.

PACS: 33, 42.65

It has been shown in recent publications that vibrational relaxation in the first excited electronic state of dye molecules may be studied measuring the nonlinear transmission of intense picosecond pulses [1, 2]. On the other hand, valuable information on molecular rotation has been obtained investigating ultrashort pulse propagation in dye solutions under different polarization conditions [3–7]. In several investigations enhanced pulse transmission was noted immediately after the occurance of the excitation pulse and a subsequent non-exponential time behaviour at short delay times of the probing light [5–7]. This time behaviour was termed coherence peak and explained by parametric four wave mixing of the laser pulses. A careful analysis of the phenomenon has been lacking.

In this letter we present theoretical and experimental data on the relevant molecular processes which determine the transmission of picosecond probing pulses in dye solutions under different polarization conditions. Our investigations reveal the importance of vibrational relaxation and of excited state absorption for an understanding of the observed signal transients. For weak excitation conditions the time evolution of the molecular system does not depend on intensity level apart from a scaling factor. The accurate knowledge of the pump pulse intensity is not required for the determination of the molecular relaxation times, if excited state absorption data are known.

1. Theory

We have performed model calculations of the molecular processes during and subsequent to an incident weak, linearly polarized excitation pulse. The following physical situation is considered (see energy level diagram of Fig. 1): Absorbing photons of energy $\hbar\omega_L$ molecules are promoted from the ground state **1** to vibrationally excited levels **2** in the S_1 state. The molecules subsequently decay to the bottom of the S_1 state **3** with vibrational relaxation time τ_v. The frequency difference between levels **2** and **3** is taken to be large compared to the homogeneous linewidth of transition **1**–**2** so that no direct pumping of level **3** occurs by the excitation pulse.

Our theoretical treatment starts from a distribution of two level systems j of transition frequencies ω_j interacting via the transition dipole moment with the excitation field ω_L. The quantum mechanical expectation value of the induced dipole moment is given by [8]

$$p_j = \frac{ia}{1 - i\,T_2(\omega_j^2 - \omega_L^2)/2\omega_L} \cdot (E_x \sin\theta\cos\phi + E_z\cos\theta) \times (1 + n_1^j - n_2^j)\,. \quad (1)$$

0721-7269/82/0027/0115/$01.60

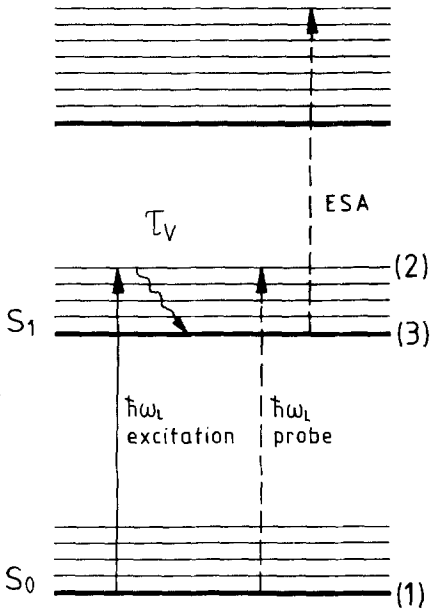

Fig. 1. Schematic of molecular transitions of the excitation (full arrows) and the probing (broken arrows) processes. Excited state absorption is negligible for the weak excitation process but notably influences the probe transmission

Equation (1) holds for quasi-stationary conditions, i.e. short values of the dephasing time T_2 as compared to the pulse duration, $T_2 \ll t_p$. This approximation is well justified for dye molecules [9] where $T_2 \sim 10^{-13}$ s and for pulses of a few picoseconds. The factor, a, collects several material constants. E_x and E_z, respectively, denote the x- and z- component of the incident light field travelling close to the y-direction. The angles θ and ϕ define the orientation of the molecular axis with respect to the laboratory frame. Molecular rotation will be treated classically on account of the large moment of inertia of dye molecules and the large damping in liquid solution. n_1^j and n_2^j denote the small population changes of levels **1** and **2**, respectively, produced by the excitation field.

Including vibrational relaxation from levels **2** to levels **3**, the excitation process is described by the rate equations:

$$\frac{\partial n_1^j}{\partial t} + \frac{n_1^j}{T_F} = id[(E_x \sin\theta\cos\phi + E_z\cos\theta)p_j^* - c.c], \tag{2}$$

$$\frac{\partial n_2^j}{\partial t} + \left(\frac{1}{\tau_v} + \frac{1}{T_F}\right) n_2^j = -\mathrm{id}[(E_x \sin\theta\cos\phi + E_z\cos\theta)p_j^* - \mathrm{c.c.}] - \frac{n_B}{\tau_v} n_1^j, \tag{3}$$

$$n_1^j + n_2^j + n_3^j = 0. \tag{4}$$

Here T_F and τ_v, respectively, are the fluorescence lifetime and the effective vibronic relaxation time; d is a coupling constant. The second term on the r.h.s. of (3) contains a Boltzmann factor $n_B \simeq \exp[-\hbar(\omega_L - \omega_0)/k_B T]$ to establish detailed balance in the S_1 levels, where $\hbar\omega_0$ is the 0–0 transition energy. $n_B \simeq 0$ is assumed in the following in agreement with our experimental situation. We now introduce the weighting factor $f(\omega_j)$ of the manifold of two level transitions $\left(\int_{-\infty}^{\infty} d\omega_j f(\omega_j) = 1\right)$ and define the average induced transition dipole moment:

$$p = ia[E_x \sin\theta\cos\phi \times E_z\cos\theta] \cdot \int_{-\infty}^{\infty} d\omega_j f(\omega_j)(1 + n_1^j - n_2^j)/[1 - iT_2(\omega_j^2 - \omega_L^2)/2\omega_L] \tag{5}$$

The mean population changes n_1 and n_2 of the lower and upper levels are derived in an analogous manner by integration over $f(\omega_j)$.

Propagation of the light pulses through the sample is governed by the nonlinear wave equation [8]. The pump pulse makes a small angle of a few degrees with the y-axis, while the probe field is taken to travel exactly in the y-direction. The pump field is linearly polarized in the z-direction; the E vector of probe light is rotated by $\gamma = 45°$ with respect to the pump field (Fig. 2). We restrict our calculations to small population changes, $|n_1| \ll 1$ and make the usual assumptions of slowly varying amplitudes and plane waves. With these approximations we obtain for the excitation pulse with field amplitude E_L the simple result:

$$\frac{\partial}{\partial y} E_L(y, t') = -b_0 \langle\cos^2\theta\rangle E_L(y, t') \tag{6}$$

where

$$b_0 = b \int_{-\infty}^{\infty} d\omega_j f(\omega_j)/[1 - iT_2(\omega_j^2 - \omega_L^2)/2\omega_L]; \tag{7}$$

y is the local coordinate in a retarded frame where $t' = t - y/v$. It should be noted that population changes leading to terms proportional to E_L^3 and higher-order terms are neglected in (6) on account of the small pump intensity. Correspondingly, the orientational distribution is unperturbed to a good approximation and the ensemble average $\langle\cos^2\theta\rangle$ is the equilibrium value $\langle\cos^2\theta\rangle = 1/3$. Eq. (6) represents Beer's law with (complex) absorption coefficient $2b_0$. This finding may be used for the determination of the distribution function $f(\omega_j)$ from experimental data. The factor b in (7) is a constant collecting several material parameters.

Application of the nonlinear wave equation yields for the amplitudes $E_{||}$ and $E_\perp$ of the probe pulse polarized parallel (z-component) and perpendicular (x-component) to the excitation field the following expressions

$$\left(\frac{\partial}{\partial y} + \frac{b_0}{3}\right) E_{||} = -\langle E\cos\theta \times [b_1(n_1 - n_2) + b_2 n_2 + b_3 n_3]\rangle \tag{8}$$

and similarly

$$\left(\frac{\partial}{\partial y}+\frac{b_0}{3}\right)E_\perp = -\langle E\sin\theta\cos\phi\times[b_1(n_1-n_2)+b_2n_2+b_3n_3]\rangle. \quad (9)$$

The brackets $\langle\rangle$ indicate orientational averages. E denotes the field amplitude along the molecular axis:

$$E=[E_L\exp(i\Delta ky)+E_{||}]\cos\theta+E_\perp\sin\theta\cos\phi. \quad (10)$$

The interaction of the probe field with the population changes n_i is represented by the absorption coefficients $b_k(k=1,2,3)$:

$$b_k(\omega_L)=b\int_{-\infty}^{\infty}d\omega_j f_k(\omega_j)[1+iT_2(\omega_j^2-\omega_L^2)/2\omega_L]^{-1}\cdot[1+T_2^2(\omega_j^2-\omega_L^2)^2/4\omega_L^2]^{-1}. \quad (11)$$

Excited state absorption starting from the induced populations n_2 and n_3 in the upper electronic level is incorporated in (8) and (9) via the factors b_2 and b_3. Different distribution functions f_k are introduced here for absorption from the ground state, $f_1=f(\omega_j)$, and from the upper electronic levels ($k=2,3$). In this way the detailed absorption properties of a molecule are taken into account. The relative magnitude of the transition dipole moments of transitions starting from levels **2** and **3** is incorporated in $f_2(\omega_j)$ and $f_3(\omega_j)$. The factor Δk on the r.h.s. of (10) denotes the wave vector mismatch $\Delta k=(\mathbf{k}_{pr}-\mathbf{k}_L)\mathbf{k}_{pr}/k_{pr}$ between the pump and probe beam.

The population changes n_1 through n_3 are evaluated here retaining terms up to second order in the pump field, E_L^2. By the help of (1) to (4) one finds

$$\frac{\partial n_1}{\partial t}+\frac{n_1}{T_F}=-d|E_{\text{eff}}|^2, \quad (12)$$

$$\frac{\partial n_2}{\partial t}+\left(\frac{1}{\tau_v}+\frac{1}{T_F}\right)n_2=d|E_{\text{eff}}|^2, \quad (13)$$

and $n_1+n_2+n_3=0$. The effective excitation field E_{eff} is given by

$$|E_{\text{eff}}|^2=|E_L|^2\cos^2\theta+[(E_L^*E_{||}\cos^2\theta+E_L^*E_\perp\sin\theta\cos\theta\cos\phi)\cdot\exp(i\Delta ky)+c.c.]. \quad (14)$$

For a solution of (8) and (9) several ensemble averages are required; e.g. $\langle\cos^2\theta n_k\rangle$. These quantities are evaluated after formal integration of (12) and (13). The following expressions emerge in the calculation

$$\begin{aligned}&\langle\cos^2\theta(t)\cos^2\theta(t')\rangle=\tfrac{1}{9}+\tfrac{4}{45}\Phi_1(t-t')\\&\langle\sin^2\theta(t)\cos^2\phi(t)\sin^2\theta(t')\cos^2\phi(t')\rangle\\&\quad=\tfrac{1}{9}+\tfrac{4}{45}\Phi_2(t-t')\\&\langle\sin^2\theta(t)\cos^2\phi(t)\cos^2\theta(t')\rangle\\&\quad=\tfrac{1}{9}-\tfrac{2}{45}\Phi_3(t-t').\end{aligned} \quad (15)$$

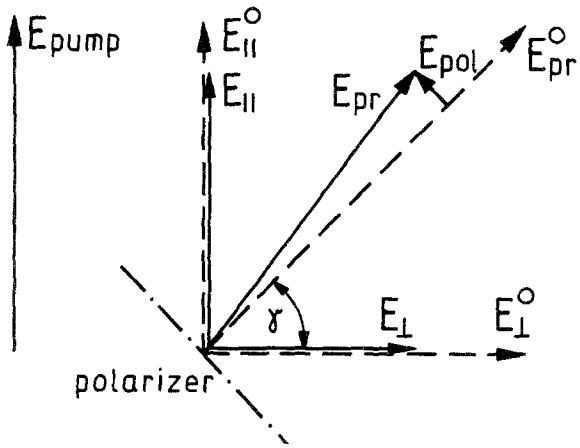

Fig. 2. Geometry of the electric field vector of the pump, incident probe field E_{pr}^o (broken arrows) and transmitted probe field E_{pr} (full arrows). E_{pol} is the probe component observed behind the analysing polarizer

Due to the weak excitation field, the ensemble averages $\langle\rangle$ refer to the equilibrium orientational distribution and the Φ_k's on the r.h.s. of (15) are functions of $|t-t'|$ only. The constant factors ascertain that the maxima at $t-t'=0$ are normalized, $\Phi_k(0)=1$. It is also known for correlation functions that $\Phi_k(\infty)=0$. For the sake of simplicity, we consider in the following the case of rotational diffusion of a molecule with identical motion about different axes. In this case a single exponential time constant describes the molecular rotation

$$\Phi_k=\exp-|t-t'|/\tau_R) \quad (16)$$

for $k=1,2,3$. τ_R denotes the rotational relaxation time. Equations (8) and (9), supplemented by (6, 12–16) allow the calculation of the probe fields $E_{||}$ and $E_\perp$. Experimentally we observe the transmitted probe pulse through the sample behind an analysing polarizer which is set at 90° with respect to the polarization of the incident probe pulse [5]. In this way the probe field in the absence of an excitation pulse is effectively blocked. For an angle γ made up by the polarization directions of the incident pump and probing pulses, the probe field behind the polarizer is given by (Fig. 2)

$$E_{\text{pol}}=[E_{||}(y,t)-E_\perp(y,t)]\sin\gamma\cos\gamma, \quad (17)$$

where a loss factor of the polarizer has been omitted. It is obvious from (17) that a polarization angle of $\gamma=45°$ gives optimum signals. The time resolution of conventional photo-detectors is not sufficient to resolve picosecond pulses. One observes a time integrated transmission signal $T(t_D)\propto\int dt|E_{\text{pol}}|^2$ of the probe pulse.

We have solved (8) and (9) and computed numerical results of the probe signal $T(t_D)$. We find that the probe transmission depends quadratically on the peak intensity I_L of the pump pulse. The result is valid for small population changes of the ground state,

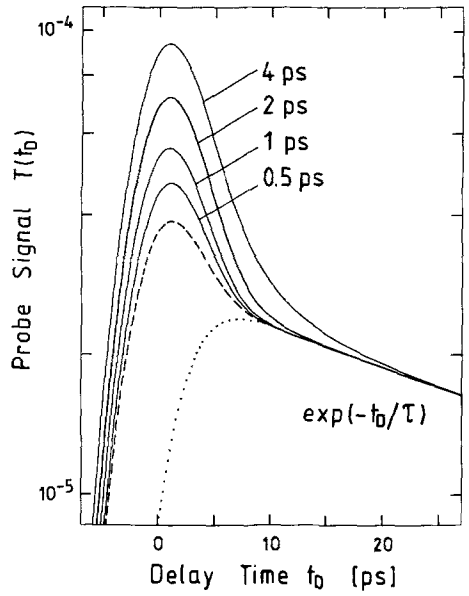

Fig. 3. Calculated probe signal $T(t_D)$ vs delay time t_D of the probe pulse for several finite values of τ_v (solid curves) and for $\tau_v=0$ (broken curve). Dotted curve: without coherence peak, see text

$|n_1| \lesssim 10^{-2}$. Such an excitation may be produced by pump pulses of $I_L \lesssim 10^7$ W/cm^2 for dye molecules with an absorption cross section of several 10^{-16} cm^2. An induced probe transmission of $T_{max} \lesssim 10^{-4}$ results for a sample transmission of $\sim 30\%$. The transient response of the molecules does not depend on the pulse intensity apart from a scaling factor. Keeping I_L constant in an experiment, the molecular time constants may be determined without the accurate knowledge of the absolute value of I_L and of the absorption cross section. This fact is highly advantageous as compared with nonlinear techniques applied recently [1].

In the following the situation $\Delta kl \gg 1$ is considered. This condition holds well for a sample length l of a few mm and an angle between probe and pump beams of a few degrees ($\Delta k \sim 10^2$ cm^{-1}). In this case the signal transients are independent of Δkl.

Some numerical examples are presented in Fig. 3. Gaussian shape is assumed for the pump and probing pulses with duration $t_p = 5$ ps. The computed ratio $T(t_D)$ of transmitted probe energy to incident pulse energy is plotted on a logarithmic scale versus time delay between probe and pump pulse. $t_D = 0$ marks the maximum of the pump pulse. The solid curves represent the data obtained for our generalized three-level system with finite vibrational lifetime τ_v. Four values, $\tau_v = 0.5$, 1, 2, and 4 ps are considered. For simplicity, excited state absorption is assumed to be absent in the Fig. 3, $b_2 = b_3 = 0$. The signal curves first rise to maxima shortly after $t_D = 0$, which depend on τ_v, and subsequently decay in two steps. We note in Fig. 3 a first rapid nonexponential decrease depending on τ_v. The later part of the signal curve displays an exponential slope with relaxation rate $1/\tau = 2/\tau_R + 2/T_F$.

It is interesting to point to the situation $\tau_v = 0$ (broken curve). The same result is also obtained (apart from a scaling factor) for a two level system where vibrational relaxation is completely omitted in the calculation. While the asymptotic time dependence of the broken curve is identical, the signal enhancement around $t_D = 0$ is significantly smaller. The small peak is due to a two-step four-wave mixing process via the electric transition dipole moment of the molecules. It represents a coherence phenomenon and may be visualized as Bragg scattering of the pump pulse by an induced grating in the sample [6, 10]. The grating is generated by population changes induced by the superposition of probe and pump field. In fact, the coherence peak of the broken curve in Fig. 3 is produced by the second term on the r.h.s. of (14) for the effective pump field. If one omits in (14) the expressions proportional to the products $E_L^* E_{\parallel}$, $E_L^* E_{\perp}$ (and c.c.), the four-wave mixing process is omitted in the computation, yielding the dotted line in Fig. 3 without a coherence peak.

There are two possible ways for the determination of the vibrational relaxation time.

(i) If $\tau_v \gtrsim t_p$, the time constant may be obtained from the nonexponential decay for small values of t_D.

(ii) For small values of the vibrational time constant ($\tau_v \lesssim t_p$), information is still available from the signal enhancement around $t_D \simeq 0$.

We introduce the peak height H as the ratio of signal maximum T_{max} to the value of the exponential asymptot at the same time $t_{D,max}$

$$H = \frac{T_{max}}{T(t_D)\exp[(t_D - t_{D,max})/\tau]}, \quad t_D \to \infty. \tag{18}$$

In the absence of vibrational relaxation, i.e. for the pure coherence phenomenon and for Gaussian pulses we calculate an enhancement of $H \simeq 1.4$. Similar numbers of H are evaluated for other pulse shapes. It is demonstrated by the curves of Fig. 3 that significantly larger peak values occur for finite vibrational relaxation times. The more pronounced signal enhancement is due to the transient population and subsequent depopulation of levels **2** during the measuring process. For example a value of $H \simeq 3$ is predicted for $\tau_v = 4$ ps in Fig. 3.

Our results on the signal enhancement for $\tau_v < t_p$ are briefly summarized as follows:

(i) The peak height increases with increasing value of τ_v.

(ii) The signal peak H does not depend on the ground state absorption constants b_0 and b_1 defined above. It is, however, influenced by the relative magnitude of the excited state absorption coefficients b_2/b_1 and b_3/b_1. Increasing b_3 leads to a larger absorption via levels **3**.

Consequently, the magnitude of the asymptotic signal is reduced and the peak height increases (note [18]).
(iii) The enhancement H of the signal is independent of the pump and probe intensity ($I_L > I_{pr}$).
Some numerical data are shown in Fig. 4. The signal enhancement H is plotted versus τ_v/t_p (lower scale) and τ_v (upper scale, $t_p = 5.0$ ps). The small value of $H \simeq 1.4$ for $\tau_v = 0$ represents the pure four-wave phenomenon. The broken curve is calculated for a situation without excited state absorption, $b_2 = b_3 = 0$. The effect of excited state absorption is demonstrated by the solid curves in Fig. 4. For simplicity we assume $b_2 \simeq b_3$ and consider transitions close to the band centers. In this case (11) yields small values of the imaginary parts of b_1, b_2, and b_3, which may be neglected. It is interesting to see that the peak height H is notably effected by the ratio of excited state to ground state absorption, b_3/b_1. For example, at $\tau_v/t_p = 0.25$ one computes $H \simeq 2.1$ for $b_3 = 0$ while $H \simeq 3.1$ is obtained for $b_3/b_1 = 0.5$. We conclude from Fig. 4 that the vibrational time constant may be deduced from the value of the peak height if the excited state absorption is known.

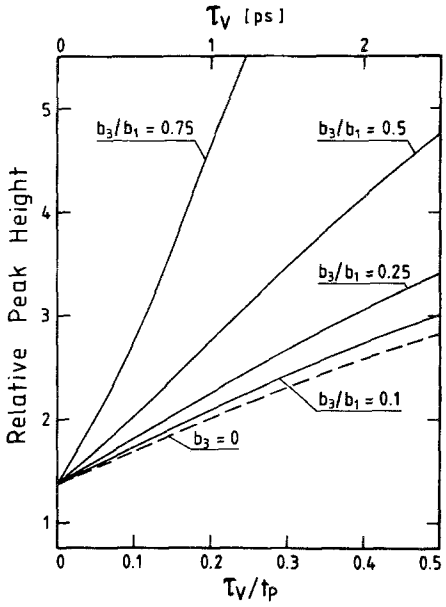

Fig. 4. Relative peak height H vs τ_v/t_p (lower scale) and τ_v (upper scale, $t_p = 5$ ps) for different values of the excited state absorption

2. Experimental Results

We have tested our theoretical results experimentally. Figure 5 gives a schematic of our experimental system. Single picosecond pulses are generated by a passively mode-locked Nd-glass laser system [11]. The pulse is selected from an early part of the pulse train, and converted to the second-harmonic frequency by a KDP crystal. The green light pulse at 527 nm has a duration of 5.0 ps as measured by correlation techniques and an energy of about 100 μJ. The green pulse is directed into the sample cell and serves as excitation pulse. A moderate intensity level of several 10 MW/cm^2 is adjusted using a large beam diameter of ~3 mm and a suitable filter. A beam splitter BS generates the weak probing pulse, which is properly attenuated by filters ($I_{pr} \simeq I_L/50$) and delayed by the help of a variable prism setup. The polarization plane of this pulse is rotated by a $\lambda/4$ plate and a first polarizer P1 to an angle of 45° relative to the excitation pulse. After the sample cell the probe pulse passes a second crossed polarizer P2, which effectively blocks the probe light. Without an excitation pulse, a large blocking factor of better than 10^7 is achieved on account of the proper alignment and the high quality of the optical components. It should be noted that no additional optical components besides the sample cell are placed between the polarizers to achieve the low background level. The probe light passing P2 is detected by a photo-multiplier. An aperture defines the small solid angle of acceptance (1×10^{-7} sr) and discriminates the stray light background of the optical system.
We have investigated the dye molecules phenoxazone 9 and rhodamine 6 G in liquid and solid solutions. The molecules are depicted in the insets of Fig. 6a and

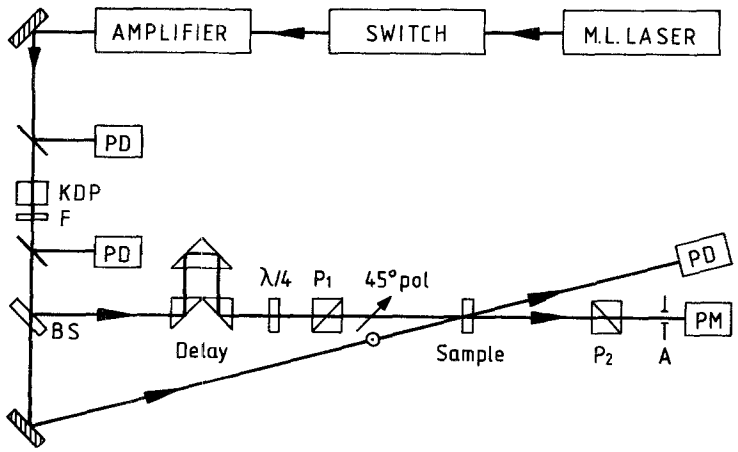

Fig. 5. Schematic of our experimental setup to measure ultrafast induced dichroism

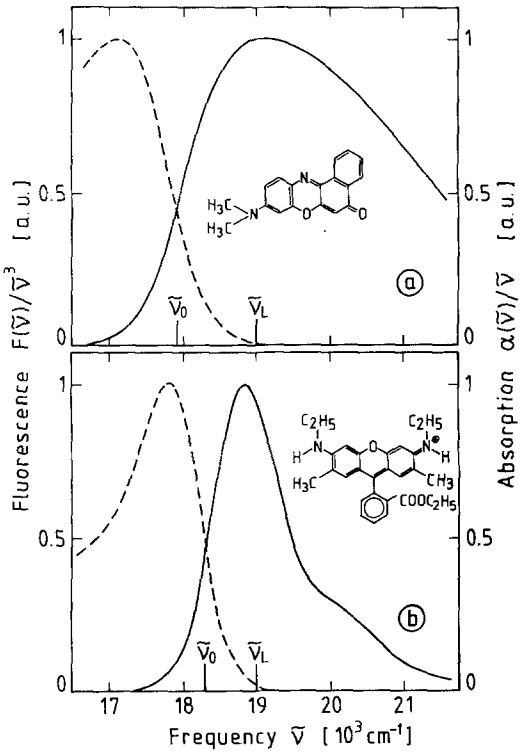

Fig. 6a and b. Absorption and fluorescence spectra of (a) phenoxazone 9 in dioxane, (b) rhodamine 6 G in ethanol. The investigated molecules are shown in the insets

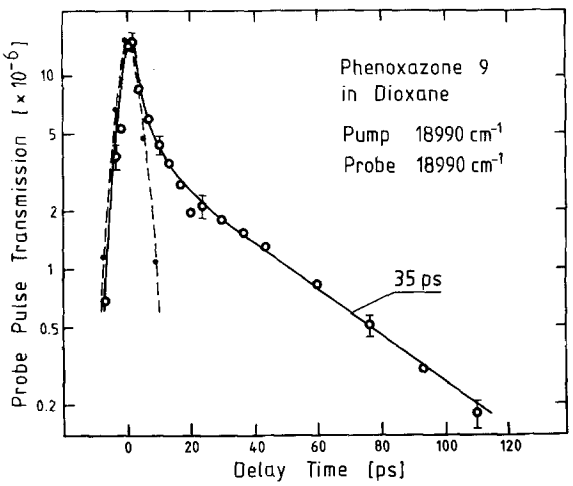

Fig. 7. Measured probe pulse transmission $T(t_D)$ vs delay time of phenoxazone 9 in dioxane. The relative peak height is found to be 4.0 ± 0.4. The broken curve shows the instrumental response of our measuring system

b. The conventional absorption (full line) and fluorescence spectra (broken curve) for phenoxazone 9 in dioxane are plotted in Fig. 6a. We estimate the 0–0 frequency from the spectroscopic data [12] to be $\tilde{\nu}_0 = 17{,}950 \pm 100\,\mathrm{cm}^{-1}$, The frequency $\tilde{\nu}_L = 18{,}990\,\mathrm{cm}^{-1}$ of the excitation and probing pulse is also indicated. By absorption of photons $\tilde{\nu}_L$ Franck Condon levels approximately $1000\,\mathrm{cm}^{-1}$ above the bottom of the S_1 are populated representing the distribution of levels **2** in our model. Vibrational relaxation will subsequently populate lower-lying levels close to the bottom of the S_1. The spectroscopic data for rhodamine 6 G in ethanol are presented in Fig. 6b. In this molecule, vibronic levels $\sim 700\,\mathrm{cm}^{-1}$ above the bottom of the S_1 state are populated by the excitation pulse. Figure 6a and b show that the upper states **2** are situated close to the maxima of the absorption bands. It is concluded that the imaginary part of b_1 may be neglected, note (11) for $k = 1$. Figs. 7–9 show several examples of ultrafast induced dichroism. Sample transmission at $\tilde{\nu}_L$ is approximately 30% corresponding to a concentration of $\sim 10^{-4}$ mol/l for phenoxazone and $\sim 2 \times 10^{-5}$ mol/l for rhodamine ($l = 2$ mm).

Our time resolved data on phenoxazone 9 and the solvent dioxane are depicted by Fig. 7. The induced probe transmission is plotted on a semi-logarithmic scale versus delay time between probe and pump pulse. The experimental points (open circles) extend over a factor of ~ 100 and represent average values of 30 to 40 individual measurements. The typical experimental error of approximately 10% is indicated. The signal points first rise to a maximum which occurs shortly after the maximum of the pump pulse ($t_D = 0$). The curve then rapidly decays giving direct evidence for fast vibrational relaxation and finally reaches an exponential asymptot with time constant $\tau = 35$ ps. Of special interest is the signal enhancement around $t_D = 0$, indicating a peak height $H = 4.0 \pm 0.4$. This value is significantly larger than the limiting value of ~ 1.4 for a "pure" coherence peak.

The instrumental response of the measuring system is shown by the broken line in Fig. 7. This curve was obtained with the identical set-up (Fig. 5) studying the pure solvent dioxane at a considerable higher intensity level. Increasing the pump intensity by a factor of ~ 50, the 4-photon interaction between the excitation and the probe pulse via the nonlinear susceptibility $\chi^{(3)}$ of the solvent molecules was studied yielding a convolution of the pump and probe pulse. The sharp increase of the pulse wings and the rapid decay is readily seen from the experimental points (full circles). The result for the pulse duration is 5.0 ps.

Our data for the solid solution of phenoxazone 9 in polystyrene are shown in Fig. 8. The signal curve rapidly rises to a maximum value with peak height $H = 2.5 \pm 0.3$ and subsequently drops to an exponential asymptot with time constant $\tau \simeq 800$ ps. We also investigated phenoxazone 9 in CCl_4. For this solution we measure a peak height $H = 1.85 \pm 0.2$ and an exponential slope with $\tau = 52$ ps.

Similar results are shown in Fig. 9 for rhodamine 6 G and the solvent ethanol. A peak height of $H = 1.8 \pm 0.2$

and an exponential slope with $\tau = 120$ ps are observed. Only part of our data on the asymptotic time dependence extending over ~300 ps are depicted in Figs. 8 and 9.

We have carefully studied the time evolution varying the pump intensity and the dye concentration. The absolute signal magnitude was found to depend quadratically on pump intensity as predicted theoretically for the intensity range considered here. The shape of the signal transients was independent of intensity. The signal curves of phenoxazone in dioxane were also measured in different concentrations in a large range of 10^{-6} to 10^{-4} mol/l. No concentration dependence was observed indicating that transition-dipole – transition-dipole interaction does not contribute to the observed exponential decay for large t_D [13]. It should be also noted that the 4-photon interaction via the nonlinear susceptibility of the solvent is completely negligible at the low intensity level used here to measure the signal transients (solid curves). It has been discussed recently that the imperfect blocking of the crossed polarizers in the experiment due to residual stress birefringence may perturb the signal transients under certain experimental conditions [7]. Our theoretical analysis for an imperfect polarizer shows that this artifact may be produced via the imaginary parts of the coefficients b_i for very small probe signals comparable to the probe background level. For our experiments with large signal to background ratio this effect is negligible. This finding demonstrates the advantage of the high power solid state laser system used here where a probe transmission level of several 10^{-5} (and even larger) is readily adjusted.

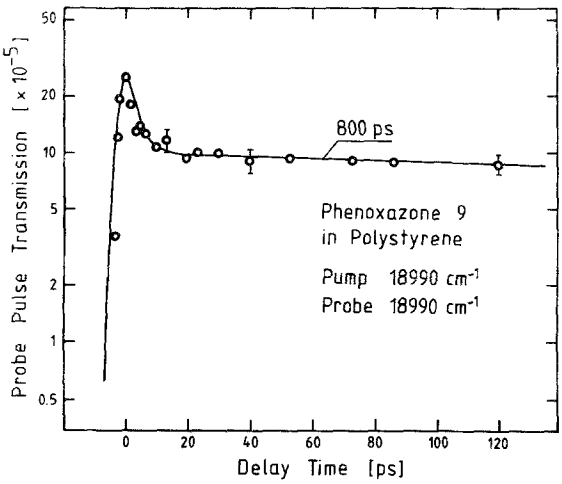

Fig. 8. Probe pulse transmission $T(t_D)$ vs delay time for the solid solution phenoxazone 9 in polystyrene. Relative peak height is 2.5 ± 0.3

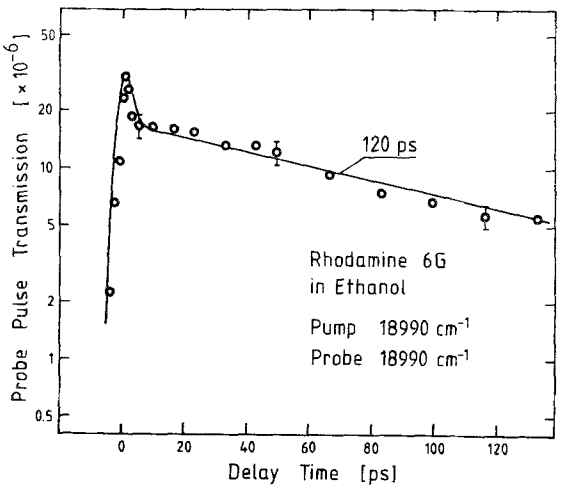

Fig. 9. Probe pulse transmission $T(t_D)$ vs delay time for rhodamine 6G in ethanol. Relative peak height is 1.8 ± 0.2

3. Discussion

We now discuss the dynamical information supplied by Figs. 7–9. In the general case the exponential slope of the signal curves is given by $1/\tau = 2/T_F + 2/\tau_R$. Comparison of Figs. 7 and 8 for phenoxazone 9 shows convincingly that the faster decay in liquid solution is generated by faster rotational relaxation in the low viscosity system ($1/\tau_R \gg 1/T_F$). In fact, a nanosecond fluorescence lifetime is expected for the highly fluorescent laser dye [14]. Application of the theory discussed above suggests a rotational relaxation time of $\tau_R \simeq 2\tau \simeq 70$ ps. A detailed investigation shows that this time constant is not the true result but represents a superposition of molecular reorientation in the S_0 and S_1 states. Molecules in the upper electronic level also contribute to the probe process via excited state absorption (Fig. 1). These data for the system phenoxazone 9 – dioxane show that molecular rotation in S_0 and S_1 is notably different [15]. In the solvent CCl_4, to the contrary, rotation in the S_0 and S_1 is similar, and $\tau = 52$ ps and our value of T_F (see below) lead to the rotational time constant $\tau_R = 110$ ps. For the solvent polystyrene the high viscosity of the solid suggests $1/\tau_R \simeq 0$. Consequently the slope with time constant $\tau \simeq 800$ ps corresponds to the fluorescence lifetime $T_F \simeq 2\tau \simeq 1.6$ ns. For rhodamine 6G in ethanol we have to take into account a long fluorescence lifetime $T_F = 3.7$ ns [16], and the slope of Fig. 9 yields $\tau_R = 250 \pm 30$ ps in good agreement with published data [4, 16, 17].

Comparison of the experimental peak heights of Figs. 7–9 with the calculated numbers of Fig. 4 allows the determination of the vibrational relaxation time. Results are shown in Table 1. We recall the large beam diameter of a few mm of the pump and probe pulses in the sample. The beam diameter is much larger than the grating constant ($\sim 10^{-3}$ cm) of the induced population grating and the plane wave approximation considered above is well justified. For the determi-

Table 1

Molecule	Solvent	b_3/b_1	Peak height	τ_v [ps]
Phenoxazone 9	Dioxane	0.75	4.0	0.8 ± 0.3
	Polystyrene	0.55	2.5	0.7 ± 0.2
	CCl_4	0.12	1.85	0.7 ± 0.2
Rhodamine 6G	Ethanol	0.1	1.8	0.5 ± 0.2

nation of τ_v we also measured the excited state absorption of phenoxazone 9 and rhodamine 6G in the solvents of interest. It should be noted that the magnitude of the excited state absorption b_2 of levels **2** is of minor importance for the determination of τ_v since these states are only weakly populated for the small values of τ_v considered here. In our experiments we find $b_2 \simeq b_3$. The imaginary part of b_3 gives rise to an ellipticity of the transmitted probe signal. An analysis of this point and a comparison of the signal magnitudes of phenoxazone 9 in the different solvents suggests that the imaginary part of b_3 gives only a minor contribution and is neglected in the following. The results on b_3/b_1 (b_1, b_3 real) are listed in the third column of Table 1 [15]. For rhodamine 6 G we find a small excited state absorption in accordance with published data [18]. With these numbers and the observed relative peak heights (fourth column) we obtain from our calculations (Fig. 4) the values of the vibrational time constant (last column of Table 1).

The solid curves in Figs. 7–9 are theoretical curves using our results on the time constants and the excited state absorption discussed above. The curve for rhodamine is calculated for the pulse duration $t_p = 4$ ps, which was used in this specific experiment. The good agreement with the experimental points should be noted.

Comparison of our data with other measurements of vibrational relaxation supports our transient dichroism technique. While phenoxazone 9 was not studied by other authors, rhodamine 6 G has been investigated by several groups with different methods. In these experiments the same excitation wavelength of 527 nm was used; i.e. the same vibronic levels were investigated. Measurements of the fluorescence risetime stated an upper limit of $\tau_v \leqq 1$ ps [19], while a nonlinear absorption technique at higher excitation level gave $\tau_v = 0.7 \pm 0.2$ ps [1]. Our result $\tau_v = 0.5 \pm 0.2$ ps at low excitation level favourably compares with these investigations. Fair agreement exists with a study of stimulated probe pulse amplification reporting $\tau_v = 2 \pm 1.4$ ps [20].

Our data for phenoxazone 9 in liquid and solid solutions do not show a solvent effect for the vibrational relaxation in the S_1 state within experimental accuracy. This result is in accordance with measurements of coumarin 7, where the vibrational relaxation in the electronic ground state was found to be independent of the solvent environment [21].

In conclusion we have theoretically studied the time evolution of induced dichroism of dye molecules. Our calculation shows that vibrational relaxation is an important factor for the observed signal transients allowing the determination of the vibrational time constant. Of particular interest is the signal enhancement during short values of delay time between probe and pump pulse. Our data represent the first measurement of vibrational time constants via ultrafast dichroism of weakly excited molecules.

We emphasize that our polarization technique does not require a precise knowledge of the absolute pump intensity since the shape of the signal transients does not depend on the intensity. The method utilizes a low pump intensity level and small population changes of the molecules. Additional processes such as excited state absorption of the pump pulse, laser emission of excited molecules and nonlinear optical processes of the solvent are negligible. In this way interpretation of the data is considerably facilitated.

Acknowledgement. The authors gratefully acknowledge the advice of Prof. H. Höcker and Dr. G. Lattermann for the preparation of the polystyrene samples.

References

1. A.Penzkofer, W.Falkenstein, W.Kaiser: Chem. Phys. Lett. **44**, 82 (1976)
2. A.Penzkofer, W.Falkenstein: Chem. Phys. Lett. **44**, 547 (1976)
3. K.B.Eisenthal, K.H.Drexhage: J. Chem. Phys. **51**, 5720 (1969)
4. T.J.Chuang, K.B.Eisenthal: Chem. Phys. Lett. **11**, 368 (1971)
5. C.V.Shank, E.P.Ippen: Appl. Phys. Lett. **26**, 62 (1975)
6. H.E.Lessing, A. von Jena, M.Reichardt: Chem. Phys. Lett. **36**, 517 (1975)
7. D.Waldeck, A.J.Cross, Jr., D.B.McDonald, G.R.Fleming: J. Chem. Phys. **74**, 3381 (1981)
8. See, for example, A.Yariv: *Quantum Electronics* (John Wiley & Sons, New York 1975)
9. H.Souma, Y.Taira, T.Yajima: In *Picosecond Phenomena*, ed. by C.V.Shank, E.P.Ippen, S.L.Shapiro (Springer, Berlin, Heidelberg, New York 1978)
10. A.von Jena, H.E.Lessing: Appl. Phys. **19**, 131 (1979)
11. D.von der Linde, O.Bernecker, W.Kaiser: Opt. Commun. **2**, 149 (1970)
    A.Laubereau, W.Kaiser: Opto-electronics **6**, 1 (1974)
12. J.B.Birks: *Organic Molecular Photophysics* (John Wiley & Sons, New York 1973)
13. K.B.Eisenthal: Chem. Phys. Lett. **6**, 155 (1970)
14. D.Basting, D.Ouw, F.P.Schäfer: Opt. Commun. **18**, 260 (1976)
15. D.Reiser, A.Laubereau: To be published
16. D.W.Phillion, D.J.Kuizenga, A.E.Siegman: Appl. Phys. Lett. **27**, 85 (1975)
17. H.J.Eichler, U.Klein, D.Langhans: Chem. Phys. Lett. **67**, 21 (1979)
18. W.Falkenstein, A.Penzkofer, W.Kaiser: Opt. Commun. **27**, 151 (1978)
19. G.Mourou, M.M.Malley: Chem. Phys. Lett. **32**, 476 (1975)
    B.Kopainsky, W.Kaiser: Opt. Commun. **26**, 219 (1978)
20. D.Ricard: J. Chem. Phys. **63**, 3841 (1975)
21. F.Wondrazek, A.Seilmeier, W.Kaiser: To be published